Cavity-induced decay of Floquet states in a bichromatic driving field

G.S. Agarwal,* W. Lange, and H. Walther
Sektion Physik der Universität München and Max-Planck-Institut für Quantenoptik, D-85748 Garching, Germany
(Received 31 March 1994; revised manuscript received 23 August 1994)

A theoretical study of the dynamics of Rydberg atoms in a microwave cavity driven by a strong bichromatic field is presented. The resonator is assumed to operate in the low-Q regime. As a consequence, photons emitted by the atoms are dissipated in the cavity walls during the interaction time of the atoms inside the resonator. In this situation the cavity field follows the atomic dynamics adiabatically. The transient behavior of the system is analyzed in terms of Floquet states and cavity-induced transition rates between these states are calculated for a large range of parameters of the bichromatic field. Narrow resonances are found in the transition rates, in agreement with recent experimental investigations of cavity Rydberg atoms subjected to strong bichromatic driving. We explain in detail the structure of the resonances, which is determined by the frequency-dependent cavity-mode density as well as the Rabi frequencies of the applied fields. The intensity-dependent shifts of the resonance frequencies are also calculated and found to be largely insensitive to inhomogeneous broadening. Finally, the numerical results are compared with experimental observations.

PACS number(s): 42.50.Ct, 42.50.Hz, 32.70.Jz, 42.52.+x

I. INTRODUCTION

Following Mollow's classic work [1] on the radiative characteristics of an atom driven by a monochromatic field, the dynamic behavior of atoms interacting with a bichromatic field has recently been studied both theoretically and experimentally. The bichromatic nature of the driving field leads to a number of new features in the field radiated by the atom that are not present in the single-frequency case. With monochromatic driving, for example, the fluorescence emitted by a two-level system shows a resonance when the excitation frequency is tuned to the atomic frequency. This resonance is power broadened when the intensity of the field is increased. In a bichromatic field, on the other hand, the fluorescence intensity exhibits well-defined resonances as a function of either the Rabi frequencies or the beat frequency of the two components of the driving field. These resonances have been verified experimentally [2,3]. Also the spectrum of fluorescence emitted by an atom in a bichromatic field is much richer than that observed in the monochromatic case [4,5]. There is a large number of sidebands, separated by the modulation frequency of the driving field amplitude. Again, experimental results agree with the theoretical predictions from Bloch equations with a bichromatic field [6,7].

It must be emphasized that existing theoretical and experimental work on resonance fluorescence in a bichromatic field is restricted to the steady-state behavior of atoms in free space. However, it was already realized in 1946 by Purcell [8] that spontaneous emission is strongly influenced by the mode density distribution of the electromagnetic environment, even if no external fields are applied. If an atom is placed in a resonant cavity, the density of modes at the transition frequency is much higher than in free space, which leads to an enhanced spontaneous emission rate. Conversely, when the cavity is detuned from the atomic resonance, decay is inhibited since there is no field mode available for the atom to interact with. Both enhancement and inhibition of spontaneous emission have been observed in the optical domain [9], with microwave transitions between highly excited Rydberg levels [10,11], as well as in the infrared spectral region [12]. When a monochromatic driving field is applied to an atom in a cavity, additional effects occur. The atomic dynamics in the presence of a frequency-dependent mode density leads to the suppression of spontaneous emission [13,14] even when the atoms and the cavity are in resonance.

The remarkable phenomena found in interactions of atoms with bichromatic fields, on the one hand, and cavity-related phenomena, on the other, provided the stimulus for the present analysis of the interplay between cavity-modified dynamics and bichromatic driving. A further motivation was the need to examine the transient behavior of atoms in the event of Rabi evolution and radiative decay being equally important [15]. Transient effects are particularly relevant to the dynamics of Rydberg atoms in cavities, where no steady state is reached during the interaction time due to the long radiative lifetimes involved.

The present work provides a theoretical interpretation of experiments at Max-Planck-Institut für Quantenoptik in Garching [16] for investigating the dynamics of Rydberg atoms in a microwave cavity driven by an intense bichromatic field. The paper is organized as follows. In Sec. II we lay the theoretical foundation for studying the cavity quantum electrodynamics of a Rydberg atom in a bichromatic field. Note that effectively one has to con-

*Permanent address: School of Physics, University of Hyderabad, Hyderabad 500 134, India.

sider the interaction of atoms with fields of frequencies ω_1, ω_2, corresponding to the two injected fields, and the cavity field at ω_c. The strong driving fields are described as classical fields, while the cavity mode has to be treated quantum mechanically. We take into account effects due to the finite cavity Q factor and temperature of the cavity walls. In this paper we only consider the limiting case of a low-Q cavity, which allows us to eliminate the cavity variables adiabatically. The periodicity of the problem makes it advantageous to analyze the system in terms of Floquet states of the atom. In Sec. III cavity-induced transition rates between the Floquet levels are calculated from the master equation. In Sec. IV we present numerical results. The origin of the resonances observed experimentally is discussed in detail. They arise from the combined effect of the dipole matrix element of transitions between Floquet states and the resonant structure of the cavity mode. Avoided crossings between the Floquet levels play a dominant role in determining the nature of the observed resonances. To obtain a realistic model of the experiment, we also include the effects of inhomogeneous broadening of the atomic line. Finally, in Sec. V the most important numerical results are compared with the experimental findings.

II. BASIC EQUATIONS FOR THE ATOMIC DYNAMICS IN A CAVITY UNDER INTENSE BICHROMATIC DRIVING

We consider a two-level atom with a transition frequency ω_0 which is coupled to a single-mode cavity of frequency ω_c. The cavity is driven by a bichromatic field with frequency components ω_1 and ω_2 and amplitudes E_1 and E_2. The detunings of the injected fields relative to the atomic levels are sketched in Fig. 1. The Hamiltonian for the interaction of the atom, the cavity mode, and external fields can be written as

$$\begin{aligned} H = {} & \hbar\omega_0 S^z + \hbar\omega_c a^\dagger a + \hbar g\left(S^+ a + S^- a^\dagger\right) \\ & + \hbar(aE_1^* e^{i\omega_1 t} + a^\dagger E_1 e^{-i\omega_1 t} \\ & + aE_2^* e^{i\omega_2 t} + a^\dagger E_2 e^{-i\omega_2 t}). \end{aligned} \tag{2.1}$$

The annihilation and creation operators a and $a^\dagger$ are associated with the cavity mode and the spin-$\frac{1}{2}$ angular momentum operators $S^\pm$ and S^z provide a description of the two-level atom. The Hamiltonian (2.1) has to be

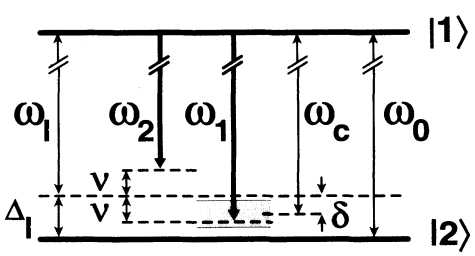

FIG. 1. Scheme of the unperturbed atomic states and the frequencies characterizing the system. The theoretical analysis uses the frame rotating at the average driving frequency ω_l. Experimental spectra are taken by scanning ω_1 across the cavity frequency ω_c (shaded region) while keeping ω_2 fixed.

supplemented to include the relaxation of the cavity with quality factor Q at a finite temperature T. The master equation describing dissipation in the combined system of atom and cavity field is

$$\begin{aligned} \frac{d\rho}{dt} &= -\frac{i}{\hbar}[H,\rho] + \mathcal{L}\rho, \\ \mathcal{L}\rho &= -\kappa(1+\bar{n})\left(a^\dagger a\rho - 2a\rho a^\dagger + \rho a^\dagger a\right) \\ &\quad -\kappa\bar{n}\left(aa^\dagger\rho - 2a^\dagger\rho a + \rho aa^\dagger\right). \end{aligned} \tag{2.2}$$

Here $\kappa = \omega_c/2Q$ is the cavity field damping rate and $\bar{n}$ is the mean thermal photon number in the cavity.

It is advantageous to transform Eq. (2.2) to a representation in which the two components of the driving field couple directly to the atom. This leaves the cavity mode with only a small average occupation of $\bar{n}$ thermal photons. We introduce the unitary displacement operator

$$D(\lambda) = \exp\left(\lambda a^\dagger - \lambda^* a\right), \tag{2.3}$$

where λ is defined as

$$\lambda = \sum_{k=1,2} \frac{E_k\, e^{-i\omega_k t}}{i\kappa - \omega_c + \omega_k}. \tag{2.4}$$

We can now set up the master equation for the transformed density matrix

$$\rho' = D^\dagger(\lambda)\rho D(\lambda), \tag{2.5}$$

which can be written as

$$\frac{d\rho'}{dt} = -\frac{i}{\hbar}[H',\rho'] + \mathcal{L}\rho' \tag{2.6}$$

if we define the Hamiltonian in the new picture as

$$\begin{aligned} H' = {} & \hbar\omega_0 S^z + \hbar\omega_c a^\dagger a + \hbar g\left(S^+ a + S^- a^\dagger\right) \\ & + \frac{\hbar}{2}\left(\Omega_1 S^+ e^{-i\omega_1 t} + \Omega_2 S^+ e^{-i\omega_2 t} + \text{H.c.}\right). \end{aligned} \tag{2.7}$$

The complex Rabi frequencies Ω_1 and Ω_2 are related to the applied field amplitudes by

$$\Omega_k = -i\frac{2gE_k}{\kappa + i(\omega_c - \omega_k)}, \qquad k = 1,2. \tag{2.8}$$

For a resonant driving field $\omega_k = \omega_c$, the intracavity Rabi frequency reaches its largest modulus

$$\Omega_k^0 = \frac{2gE_k}{\kappa}, \qquad k = 1,2. \tag{2.9}$$

The driving term in the Hamiltonian H' is periodic in time, the modulation frequency being $2\nu = \omega_2 - \omega_1$. Even though no stationary eigenstates of H' exist, applying Floquet's theorem [17] allows solutions of the Schrödinger equation to be expanded in a series of terms oscillating at harmonics of frequency ν. The associated energy levels are called Floquet levels or quasienergy levels. As they constitute a natural basis for the treatment of bichromatic interactions, the system will be analyzed in terms of Floquet states of H'. We are mainly interested in the

change of atomic inversion in the Floquet basis, since this is the quantity monitored in the Rydberg atom experiment of Lange, Walther, and Agarwal [16]. It is assumed that the atoms enter the cavity adiabatically, so that Landau-Zener-type transitions between the Floquet states during entry and exit can be neglected. In this case the principal source of decay of atomic inversion are cavity-induced transitions among the Floquet states. In the transient regime we consider, the relevant quantity is the rate at which these transitions occur.

A. Floquet basis

First we consider the Hamiltonian H_0 in the absence of the cavity field:

$$H_0 = \hbar\omega_0 S^z + \frac{\hbar}{2}\left(\Omega_1 S^+ e^{-i\omega_1 t} + \Omega_2 S^+ e^{-i\omega_2 t} + \text{H.c.}\right). \tag{2.10}$$

We will work in a frame rotating at the average driving field frequency

$$\omega_l = \frac{\omega_1 + \omega_2}{2}. \tag{2.11}$$

The effective Hamiltonian in the rotating frame is

$$H_e = \hbar\Delta_l S^z + \frac{\hbar}{2}\left[S^+(\Omega_1 e^{i\nu t} + \Omega_2 e^{-i\nu t}) + \text{H.c.}\right], \tag{2.12}$$

where $\Delta_l = \omega_0 - \omega_l$. The unperturbed states of the atom with energies $\hbar\omega_0/2$ and $-\hbar\omega_0/2$ are denoted as $|1\rangle$ and $|2\rangle$, respectively. Making use of the periodicity of $H_e(t)$, we apply Floquet's theorem [17,18] to solve the Schrödinger equation

$$i\hbar\frac{\partial}{\partial t}|\Psi(t)\rangle = H_e(t)\,|\Psi(t)\rangle. \tag{2.13}$$

Solutions of Eq. (2.13) are the so-called quasienergy wave functions $|\Psi(t)\rangle$, defined by the series expansion

$$|\psi(t)\rangle = e^{-iEt}\sum_{n=-\infty}^{\infty}\left(\alpha_{1n}|1\rangle + \alpha_{2n}|2\rangle\right)e^{-in\nu t}. \tag{2.14}$$

The eigenvalues E and the eigenvector components α_{in} are determined by inserting expansion (2.14) into (2.13), yielding the recurrence relations

$$\left(E + n\nu - \frac{\Delta_l}{2}\right)\alpha_{1n} = \alpha_{2,n-1}\frac{\Omega_2}{2} + \alpha_{2,n+1}\frac{\Omega_1}{2},$$
$$\left(E + n\nu + \frac{\Delta_l}{2}\right)\alpha_{2n} = \alpha_{1,n-1}\frac{\Omega_1^*}{2} + \alpha_{1,n+1}\frac{\Omega_2^*}{2}. \tag{2.15}$$

These are then solved by standard continued fraction methods [19,20]. It should be noted that

$$\sum_n(\alpha^*_{1,p+n}\alpha_{1n} + \alpha^*_{2n}\alpha_{2,p+n}) = \delta_{p0}. \tag{2.16}$$

This follows from our choice of the energies of the unperturbed states and the normalization $\langle\psi|\psi\rangle = 1$. Note further that if E is an eigenvalue, $\pm E + n\nu$ is also an eigenvalue. It is therefore sufficient to calculate the lowest positive eigenvalue, which we will call ϵ. From the periodicity of the quasienergies it follows that $2\epsilon < \nu$.

We now make a specific choice of the basis states for determining cavity-induced transition rates. We use the two adjacent Floquet states with quasienergies $\pm\epsilon$ at the time $t = 0$:

$$|\psi_\pm\rangle \equiv |\psi_{E=\pm\epsilon}(t=0)\rangle \equiv \sum_n\left(\alpha_{1n\pm}|1\rangle + \alpha_{2n\pm}|2\rangle\right). \tag{2.17}$$

The thermal cavity field at the finite temperature T and spontaneous emission cause transitions between the Floquet states $|\psi_+\rangle$ and $|\psi_-\rangle$. We will calculate the corresponding cavity-modified transition probability.

B. Adiabatic elimination of the cavity field

The cavity-induced transition rate between the basis states $|\psi_\pm\rangle$ may be calculated on the assumption that the cavity Q is low enough for the cavity variables to be adiabatically eliminated. Throughout this paper we will work in this limit. Defining

$$\delta = \omega_c - \omega_l, \tag{2.18}$$

Eq. (2.2) is rewritten in the rotating frame:

$$\frac{d\rho'}{dt} = -\frac{i}{\hbar}\left[H_e + \hbar\delta_c a^\dagger a + \hbar g\left(S^+ a + S^- a^\dagger\right), \rho'\right] + \mathcal{L}\rho'. \tag{2.19}$$

We now make a transformation to the interaction picture so that

$$\tilde{\rho}'(t) = e^{-\mathcal{L}t}\left[e^{i\delta_c a^\dagger a\, t}U_e^+(t)\rho'(t)U_e(t)e^{-i\delta_c a^\dagger a\, t}\right], \tag{2.20}$$

where

$$U_e(t) = T\exp\left[-\frac{i}{\hbar}\int_0^t H_e(\tau)d\tau\right], \tag{2.21}$$

T denoting time ordering. The equation of motion for $\tilde{\rho}'$ is found to be

$$\frac{d\tilde{\rho}'}{dt} = -ig\left[a(t)G(t)e^{-i\delta t} + \text{H.c.}, \tilde{\rho}'\right], \tag{2.22}$$

$$a(t) = e^{-\mathcal{L}t}ae^{\mathcal{L}t}, \tag{2.23}$$

$$G(t) = U_e^+(t)S^+U_e(t). \tag{2.24}$$

Let σ be the reduced density matrix for the atomic system

$$\sigma(t) = \text{Tr}_{\text{cavity}}\,\tilde{\rho}'(t). \tag{2.25}$$

Following the method presented in Appendix A of Ref. [21], we derive the master equation for $\sigma(t)$, assuming that the cavity field can be adiabatically eliminated:

$$\frac{d\sigma}{dt} = -g^2(1+\bar{n})\int_0^\infty d\tau\, e^{-\kappa\tau - i\delta\tau}[G(t)G^+(t-\tau)\sigma - G^+(t-\tau)\sigma G(t)] - g^2\bar{n}\int_0^\infty d\tau\, e^{-\kappa\tau - i\delta\tau}[\sigma G^+(t-\tau)G(t) - G(t)\sigma G^+(t-\tau)] + \text{H.c.} \quad (2.26)$$

The density matrix equation in the original picture is obtained by applying the unitary transformation (2.21). The solution of Eq. (2.26) yields complete information on the atomic dynamics. However, it can only be obtained numerically because of the explicit time dependence of the Hamiltonian $H_e(t)$ [Eq. (2.12)].

III. MASTER EQUATION IN THE FLOQUET BASIS

In this section we calculate the cavity-induced transition rates between Floquet states. Equation (2.26) is used to derive a Pauli-like master equation for the diagonal elements of the atomic density matrix, projected to the Floquet basis $|\psi_\pm\rangle$ defined in Eq. (2.17). We make the secular approximation, assuming that the diagonal and off-diagonal terms do not couple, to obtain an equation for the evolution of the Floquet populations:

$$\dot{\sigma}_{++} = -\Gamma_+\sigma_{++} + \Gamma_-\sigma_{--}, \quad (3.1)$$

$$\dot{\sigma}_{--} = -\Gamma_-\sigma_{--} + \Gamma_+\sigma_{++}, \quad (3.2)$$

$$\sigma_{\pm\pm} = \langle\psi_\pm|\sigma|\psi_\pm\rangle. \quad (3.3)$$

The rates Γ_+ (Γ_-) thus describe cavity-induced transitions from $|\psi_+\rangle$ to $|\psi_-\rangle$ ($|\psi_-\rangle$ to $|\psi_+\rangle$). The secular approximation is justified as long as the levels $|\psi_+\rangle$ and $|\psi_-\rangle$ are not degenerate and breaks down only in the limit $\epsilon \to 0$.

Using Eq. (2.26), we determine the rates $\Gamma_\pm$ as

$$\Gamma_+ = \int_0^\infty \{g^2(1+\bar{n})\left[\langle\psi_+|G(t)G^+(t-\tau)|\psi_+\rangle - \langle\psi_+|G^+(t-\tau)|\psi_+\rangle\langle\psi_+|G(t)|\psi_+\rangle\right] + g^2\bar{n}\left[\langle\psi_+|G^+(t-\tau)G(t)|\psi_+\rangle - \langle\psi_+|G(t)|\psi_+\rangle\langle\psi_+|G^+(t-\tau)|\psi_+\rangle\right]\} d\tau\, e^{-\kappa\tau - i\delta\tau} + \text{c.c.}, \quad (3.4a)$$

$$\Gamma_- = \int_0^\infty \{g^2(1+\bar{n})\left[\langle\psi_-|G(t)G^+(t-\tau)|\psi_-\rangle - \langle\psi_-|G^+(t-\tau)|\psi_-\rangle\langle\psi_-|G(t)|\psi_-\rangle\right] + g^2\bar{n}\left[\langle\psi_-|G^+(t-\tau)G(t)|\psi_-\rangle - \langle\psi_-|G(t)|\psi_-\rangle\langle\psi_-|G^+(t-\tau)|\psi_-\rangle\right]\} d\tau\, e^{-\kappa\tau - i\delta\tau} + \text{c.c.} \quad (3.4b)$$

Only the constant components of the transition rates will be retained. To simplify expressions (3.4), some intermediate steps are necessary. First we make use of the completeness of the Floquet basis to factor the correlation function:

$$\langle\psi_+|G(t)G^+(t-\tau)|\psi_+\rangle = \langle\psi_+|G(t)|\psi_+\rangle\langle\psi_+|G^+(t-\tau)|\psi_+\rangle + \langle\psi_+|G(t)|\psi_-\rangle\langle\psi_-|G^+(t-\tau)|\psi_+\rangle. \quad (3.5)$$

We then apply definitions (2.14), (2.21), and (2.24) to obtain

$$\begin{aligned}\langle\psi_+|G(t)|\psi_-\rangle &= \langle\psi_+|U_e^+(t)S^+U_e(t)|\psi_-\rangle \\ &= \langle\psi_+(t)|S^+|\psi_-(t)\rangle \\ &= \langle\psi_+(t)|\sum_n e^{-iE_-t - in\nu t}\alpha_{2n-}|1\rangle \\ &= e^{i(E_+-E_-)t}\sum_{n,m}\alpha_{2n-}\alpha^*_{1m+}e^{-i\nu t(n-m)}.\end{aligned} \quad (3.6)$$

Inserting Eqs. (3.6) and (3.5) into Eq. (3.4a), we find the result for the transition rate Γ_+,

$$\Gamma_+ = 2g^2(1+\bar{n})\,\mathrm{Re}\sum_{n,m,p,q}\frac{\alpha_{2n-}\alpha^*_{1m+}\alpha^*_{2p-}\alpha_{1q+}}{\kappa + i\delta - 2iE_+ + i\nu(p-q)}\times\delta_{n-m;p-q} + 2g^2\bar{n}\,\mathrm{Re}\sum_{n,m,p,q}\frac{\alpha_{2n+}\alpha^*_{1m-}\alpha^*_{2p+}\alpha_{1q-}}{\kappa + i\delta + 2iE_+ + i\nu(p-q)}\times\delta_{n-m;p-q}. \quad (3.7)$$

The rate Γ_- is obtained from Eq. (3.7) by interchanging the terms scaling with $\bar{n}$ and $1+\bar{n}$.

Next, we calculate the rate of cavity-induced decay of coherence in the Floquet basis. We continue to apply the secular approximation, so that the diagonal matrix elements σ_{++} and σ_{--}, as well as the counterrotating coherence σ_{-+}, do not appear in the equation of motion for σ_{+-}:

$$\dot{\sigma}_{+-} = -\Gamma_\perp\sigma_{+-}. \quad (3.8)$$

From Eq. (2.26) the decay rate $\Gamma_\perp$ is found to be

$$\Gamma_\perp = g^2\,\mathrm{Re}\left\{(1+\bar{n})\left[\hat{U}(\kappa+i\delta) + \hat{W}(\kappa-i\delta)\right] + \bar{n}\left[\hat{V}(\kappa+i\delta) + \hat{Z}(\kappa-i\delta)\right]\right\}, \quad (3.9)$$

where $\hat{f}$ denotes the Laplace transform of $f(\tau)$. The functions U, V, W, and Z are defined by

$$\begin{aligned}U(\tau) &\doteq \langle\psi_+|G(t)G^+(t-\tau)|\psi_+\rangle - \langle\psi_+|G^+(t-\tau)|\psi_+\rangle\langle\psi_-|G(t)|\psi_-\rangle, \\ V(\tau) &\doteq \langle\psi_-|G^+(t-\tau)G(t)|\psi_-\rangle - \langle\psi_+|G(t)|\psi_+\rangle\langle\psi_-|G^+(t-\tau)|\psi_-\rangle, \\ W(\tau) &\doteq \langle\psi_-|G(t-\tau)G^+(t)|\psi_-\rangle - \langle\psi_+|G^+(t)|\psi_+\rangle\langle\psi_-|G(t-\tau)|\psi_-\rangle, \\ Z(\tau) &\doteq \langle\psi_+|G^+(t)G(t-\tau)|\psi_+\rangle - \langle\psi_+|G(t-\tau)|\psi_+\rangle\langle\psi_-|G^+(t)|\psi_-\rangle,\end{aligned} \quad (3.10)$$

where $\doteq$ indicates that only the constant components

with respect to time t are to be retained on the right-hand sides. The explicit expression for $\Gamma_\perp$ in terms of the eigenvector components $\alpha_{kn\pm}$ of the quasistates is rather involved and so is not given here.

Experimentally, it is not the individual transition rates $\Gamma_\pm$ between the Floquet states that are observed, but the decay of the inversion $\sigma_{++} - \sigma_{--}$ in the Floquet basis, obeying the equation

$$\frac{d}{dt}(\sigma_{++} - \sigma_{--}) = -(\Gamma_+ + \Gamma_-)(\sigma_{++} - \sigma_{--}) - \Gamma_+ + \Gamma_-. \quad (3.11)$$

We will therefore concentrate on the decay rate

$$\Gamma_\parallel = \Gamma_+ + \Gamma_-, \quad (3.12)$$

which is the analog of the longitudinal relaxation rate in the standard Bloch equations.

By using Eq. (3.7) the transition rate $\Gamma_\parallel$ can be written in terms of the Floquet eigenvector components:

$$\Gamma_\parallel = 2g^2(1+2\bar{n}) \times \mathrm{Re} \sum_{n,m,p,q} \left(\frac{\alpha_{2n-}\alpha^*_{1m+}\alpha^*_{2p-}\alpha_{1q+}}{\kappa + i\delta - 2iE_+ + i\nu(p-q)} + \frac{\alpha_{2n+}\alpha^*_{1m-}\alpha^*_{2p+}\alpha_{1q-}}{\kappa + i\delta + 2iE_+ + i\nu(p-q)} \right) \delta_{n-m,p-q}. \quad (3.13)$$

Equation (3.13) is the central result of our analysis, allowing us to study cavity-induced decay of the population difference in the Floquet basis. In Sec. IV we evaluate $\Gamma_\parallel$ numerically.

Some general conclusions on $\Gamma_\parallel$ can already be obtained from the structure of expression (3.13). The sum over the product of eigenvector components in the numerator is proportional to the time-independent component of the free space fluorescence rate. Information on this quantity can be obtained from the behavior of the eigenvalues $E_\pm$ of the periodic Hamiltonian as a function of the driving field frequencies ω_1 and ω_2 [22]. It is known that fluorescence peaks when the slope of the quasienergy $E_\pm(\omega_1, \omega_2)$ approaches zero. With ω_1 as the variable frequency, this condition reads

$$\frac{\partial E_\pm}{\partial \omega_1} = 0. \quad (3.14)$$

It is met at avoided crossings of the Floquet levels. Consequently, a maximum contribution of the numerator to the decay rate $\Gamma_\parallel$ in Eq. (3.13) is expected when the quasienergy levels undergo an avoided crossing.

A nonzero dipole coupling only occurs when $P = p - q$ is an even number. Therefore, in second-order perturbation theory, only transitions with even P contribute to fluorescence. If, however, terms up to order g^4 are included in the calculation of the transition rate, resonances generated by *multiwave* mixing can occur. They are found at either avoided crossings or crossings of the Floquet levels, the latter corresponding to nonzero matrix elements involving odd values of P.

Next, modifications of the system behavior due to the presence of the cavity are to be considered. The influence of the resonant structure of the cavity response function on atomic fluorescence is expressed by the denominators in (3.13). The transition rate $\Gamma_\parallel$ exhibits cavity-induced resonances at the frequencies given by

$$\delta \pm 2\epsilon + P\nu = 0, \quad (3.15)$$

where again $P = p - q$ is an integer and $\epsilon = |E_\pm|$. As P may assume different values, several adjacent resonances may contribute to cavity-enhanced transitions. If condition (3.15) is not fulfilled, cavity-induced decay is dynamically suppressed by the bichromatic driving field. This effect is analogous to the dynamic suppression of spontaneous emission by a monochromatic field [13,14,21].

Equation (3.15) may be rewritten as

$$\omega_1 \frac{(1+P)}{2} + \omega_2 \frac{(1-P)}{2} - \omega_c = \pm 2\epsilon. \quad (3.16)$$

We are interested in the avoided crossing regions, where the numerator of $\Gamma_\parallel$ is large. Here it is advantageous to define a quantity η as the energy splitting between two Floquet levels undergoing an avoided crossing:

$$\eta \equiv |\nu| - 2\epsilon = \frac{1}{2}|\omega_2 - \omega_1| - 2\epsilon. \quad (3.17)$$

By definition, $|\eta|$ reaches its minimum at the avoided crossing. For simplicity we choose $\omega_1 > \omega_2$. Moreover, we assume that ω_1 is tuned close to the cavity frequency ω_c, as is the case in the experiment (see also Fig. 1). The reason is that only close to the cavity frequency is it possible to inject a sufficient intensity into the resonator. With definition (3.17), condition (3.16) becomes

$$\omega_c - \omega_1 + \nu P = -\eta, \quad (3.18a)$$

$$\omega_c - \omega_1 + \nu(P-2) = \eta. \quad (3.18b)$$

Thus, with $\omega_1 > \omega_c$ ($\omega_1 < \omega_c$) the cavity enhances atomic decay for $P = 0$ ($P = 2$) exclusively. The appearance of exactly these two values of P is a consequence of the choice of $|\psi_+\rangle$ and $|\psi_-\rangle$ as basis states. If other Floquet levels had been used as final and initial states, different values of P would lead to enhancement. Generally, Eqs. (3.18) show that a resonance occurs when ω_1 is tuned to $\omega_c \pm \eta$. Therefore, the splitting between the Floquet levels can be read off from the detuning between the resonance frequency ω_1 and the cavity frequency ω_c, which are easily obtained from experiment.

Peaks in the decay rate $\Gamma_\parallel$, which are large enough to be detected experimentally, can only occur if strong coupling between the Floquet levels coincides with cavity enhancement at the corresponding transition frequency. In other words, the conditions (3.14) and (3.15) must be fulfilled simultaneously. Otherwise dynamic suppression of Floquet transitions prevails and decay is inhibited. The exact position of the cavity-enhanced maxima in the decay rate can only be found numerically. However, as shown above, at resonance the detuning $|\omega_1 - \omega_c|$ is equal to the splitting η of the Floquet levels. As a con-

sequence, the location of the largest peaks in $\Gamma_{\parallel}$ yields the level splitting precisely at an avoided crossing.

Note that the quasienergies $E_{\pm}$ appearing in conditions (3.14) and (3.15), and hence η, depend on (i) the intracavity Rabi frequencies Ω_1 and Ω_2 of the two driving fields and (ii) the frequencies ω_1 and ω_2. Owing to Eq. (2.8), for given external field amplitudes E_1,E_2 the Rabi frequencies also depend on tuning and the line width κ of the cavity. We finally mention that the rate $\Gamma_{\perp}$ has additional resonances given by

$$\delta + P\nu = 0, \tag{3.19}$$

which may be rewritten as

$$\omega_c + \frac{\omega_2}{2}(P-1) - \frac{\omega_1}{2}(P+1) = 0. \tag{3.20}$$

IV. NUMERICAL RESULTS

We have studied numerically the behavior of the transition rates $\Gamma_{\parallel}$ and $\Gamma_{\perp}$ for a large range of parameters of the bichromatic field and the cavity tuning. In this section we present the main results of the analysis.

In the numerical evaluation of the decay rate we proceeded as follows. We start by determining the quasienergy ϵ. It can be obtained from the two scalar recurrence relations (2.15) by calculating the corresponding infinite continued fraction. We employed downward iteration from a suitably chosen cutoff. In a second step the eigenvector components α_{kn} are obtained, again from a continued fraction. The result is used to evaluate $\Gamma_{\parallel}$ and $\Gamma_{\perp}$.

A. Structure of resonances in the cavity-induced decay rate

As explained in Sec. III, the resonances in the decay rate are determined by the energies of the Floquet states as well as their wave functions. This is illustrated by our numerical results. Figure 2 shows the structure of the Floquet quasienergy spectrum as a function of the detuning Δ_1 of the first component of the driving field, which is the quantity scanned in the experiment. The detunings used in the numerical calculations are defined with respect to the atomic transition frequency ω_0:

$$\Delta_1 = \omega_0 - \omega_1, \qquad \Delta_2 = \omega_0 - \omega_2, \qquad \Delta_c = \omega_0 - \omega_c. \tag{4.1}$$

As noted in Sec. II A, the eigenvalue structure is periodic. The energy levels recur, raised or lowered in steps equal to the frequency ν. The slope of the levels is mainly determined by the shape of the Lorentzian cavity line. Approaching the cavity resonance, there is an increasing number of level crossings and avoided crossings. The levels cross at $E = \pm N\nu$ with integer N. At these eigenvalues, the derivative $\partial E/\partial\Delta_1$ has a local maximum and therefore the dipole transition probability is low [22]. In addition, for $\Delta_1 \approx \Delta_c$ and hence $\delta \approx -\nu$, Eq. (3.15) shows that only transitions with $P = 1$ are enhanced by the cavity when $\epsilon = 0$. As these do not correspond to possible dipole transitions, no substantial decay can occur at the level crossings.

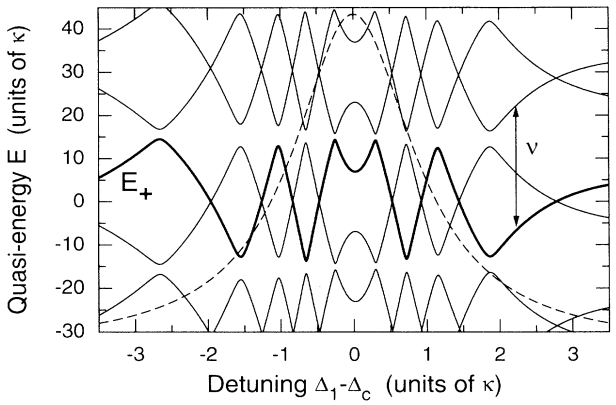

FIG. 2. Quasienergy levels of the Hamiltonian (2.12) in the Floquet picture. The energy of Floquet state $|\Psi_+\rangle$ is indicated by the thick line. The variation of the levels with detuning and the width of the avoided crossings depend on the cavity line shape (dashed line) due to the resonant enhancement of the intracavity field at ω_c. Parameters: $\Omega_1^0 = 500\kappa$, $\Omega_2^0 = 16\,255\kappa$, $\Delta_2 = 200\kappa$, and $\Delta_c = 140\kappa$.

By analogy with free-space fluorescence under bichromatic driving, which displays maxima when condition (3.14) is met, cavity-induced decay is expected to peak at avoided crossings of the quasienergy levels. These occur when ϵ approaches $\nu/2$, since this is where the level splitting η reaches a minimum. Figure 3 shows (a) two adjacent avoided crossings of the Floquet levels as well as (b) the dominant eigenvector components $\alpha_{kp\pm}$ of $|\Psi_+\rangle$ and $|\Psi_-\rangle$. It is obvious that the structure of the eigenvectors undergoes a significant change at the avoided crossing. The reason is that each of the levels involved picks up a contribution from the other level. In Fig. 3(c) the expression $|\alpha^*_{2p-}\alpha_{1p+}|^2$ is plotted, which equals the squared matrix element, taken between the p-photon components of initial state $|\Psi_+\rangle$ and final state $|\Psi_-\rangle$. In the narrow transition regions centered at the avoided crossings, this quantity has sharp maxima, since it is the product of a rising and a falling eigenvector component.

The transition from $|\Psi_+\rangle$ to $|\Psi_-\rangle$ can occur via several multiphoton processes distinguished by the number of photons at frequencies ω_1 and ω_2 being absorbed or emitted. While in free space they can equally contribute to the overall decay rate, the cavity mode resonantly enhances only a small number of multiphoton transitions, the others being strongly suppressed. It is therefore important to consider the transition matrix element as a function of the Floquet indices p and q, the number of driving field quanta associated with the final and initial states. A typical distribution of partial transition probabilities at an avoided crossing is displayed in Fig. 4. The maximum contribution comes from the transition $p = 7, q = -7$, corresponding to a process where seven photons of frequency ω_1 are absorbed and seven photons

of frequency ω_2 are emitted. In this case $P = p - q = 14$. It is apparent, for example, from Eq. (3.18), that the corresponding transition is highly nonresonant with the cavity under the experimental conditions considered. As demonstrated in Sec. III, only for $P = 0$ and $P = 2$ can resonances occur with ω_1 close to the cavity. Therefore, in Fig. 4 only the main diagonal ($p = q$) and the second subdiagonal ($p = q + 2$) have to be considered for cavity-induced decay under bichromatic driving. The corresponding partial transition matrix elements also peak at avoided crossings and quickly decrease when ω_1 is detuned.

The cavity not only selects the order of multiphoton processes contributing to a given resonance, but also determines the degree of enhancement or inhibition of spontaneous decay. The largest possible transition rate is achieved when the resonance denominator in Eq. (3.13) reaches its minimum value κ exactly at a maximum of the numerator of $\Gamma_{\|}$. For a $P = 0$ resonance [see Eq. (3.18a)], the cavity detuning δ must equal 2ϵ precisely at an avoided crossing of the energy levels. This is the case in Fig. 5(a), where ϵ and the adjacent quasienergy level are plotted as functions of the detuning Δ_1 of the first driving field, together with the cavity detuning parameter $\delta/2$. The decay rates $\Gamma_{\|}$ and $\Gamma_{\perp}$ shown in Fig. 5(b) have a strong peak when a Floquet transition is in resonance with the cavity. At this point, in Fig. 5(a) the dashed lines touch the quasienergy levels. The size of the decay rate reaches 10% of $2g^2/\kappa$, the enhanced decay rate of an atom in a cavity with no driving fields applied. Note that the peak occurs at a driving field frequency $\Delta_1 = \Delta_c - \eta$, where η is again the level splitting at the avoided crossing.

At an avoided crossing, Eqs. (3.18) can be fulfilled ex-

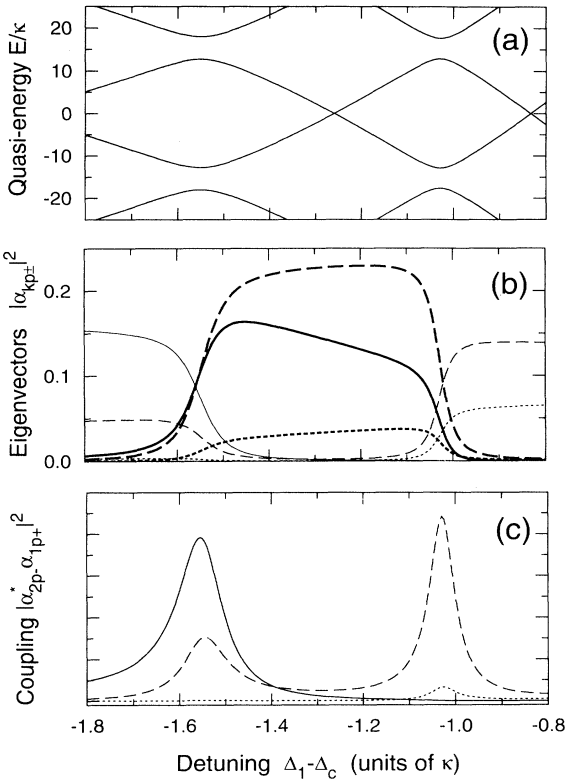

FIG. 3. (a) Two adjacent avoided crossings of the quasienergy levels. (b) Dominant eigenvector components $|\alpha_{1p+}|^2$ (thin lines) and $|\alpha_{2p-}|^2$ (thick lines) for $p = 7$ (solid), $p = 9$ (dashed), and $p = 11$ (dotted). (c) Partial transition matrix elements $|\alpha^*_{2p-}\alpha_{1p+}|^2$. The parameters are the same as those of Fig. 2.

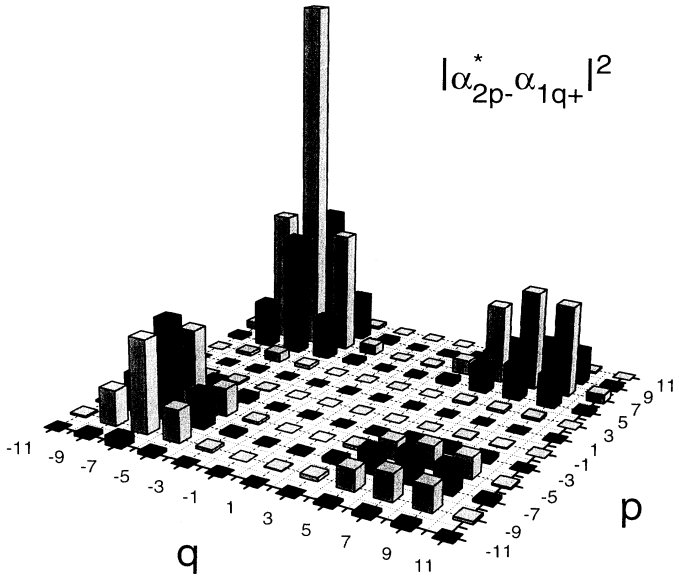

FIG. 4. Partial transition probabilities between states with p and q driving field photons. In the $|\Psi_{\pm}\rangle$ basis and for $\Delta_1 < \Delta_c$, the cavity enhances spontaneous transitions only along the diagonal ($p = q$), while all other contributions are suppressed. Parameters: $\Omega_1^0 = 6913.5\kappa$, $\Delta_1 = 93.69\kappa$, $\Omega_2^0 = 60\,000\kappa$, $\Delta_2 = 254\kappa$, and $\Delta_c = 100\kappa$.

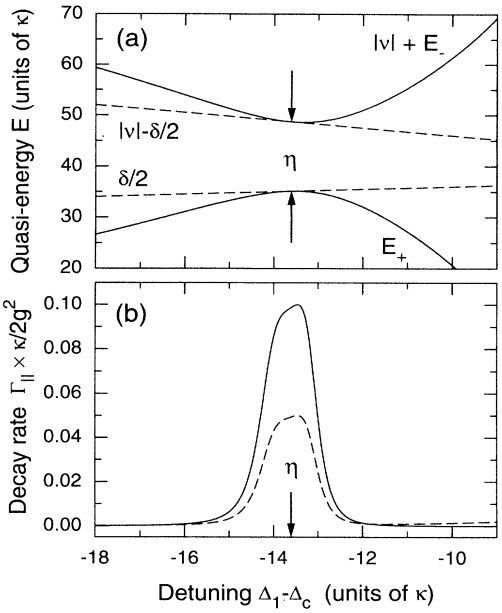

FIG. 5. (a) Quasienergy levels (solid lines) and cavity resonance (dashed lines). The latter changes with frequency ω_1 owing to the dependence of δ on ω_1 in the frame rotating with ω_l. (b) Strong peak in the cavity-induced decay rates $\Gamma_{\|}$ (solid) and $\Gamma_{\perp}$ (dashed), occurring when the cavity is tuned to resonance with an avoided crossing of the Floquet levels. Note that at the peak $|\Delta_1 - \Delta_c| = \eta$. Parameters: $\Omega_1^0 = 2350\kappa$, $\Omega_2^0 = 60\,000\kappa$, $\Delta_2 = 254\kappa$, and $\Delta_c = 100\kappa$.

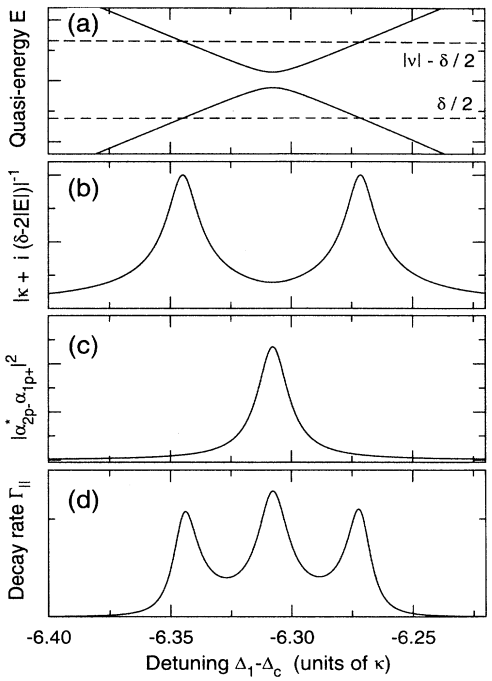

FIG. 6. Triplet structure of the decay rate $\Gamma_{\|}$ when the cavity resonance is slightly detuned from an avoided crossing. (a) Quasienergy levels (solid) and cavity resonance (dashed). (b) Cavity resonance factor $1/|\kappa + i(\delta - 2|E|)|$. (c) Transition matrix element $|\alpha^*_{2\mathrm{p}-}\alpha_{1\mathrm{p}+}|^2$. (d) Decay rate $\Gamma_{\|}$. The two side resonances correspond to the intersections of dotted and solid lines in (a). The parameters are the same as those of Fig. 4.

actly for specific parameters only. Otherwise the decay rate is less strongly enhanced or even completely suppressed. Two cases can be distinguished. Restricting the discussion to $\Delta_1 < \Delta_c$ and therefore $P = 0$, we first consider the case $\delta > 2\epsilon$ at the avoided crossing. In this situation condition (3.18a) can neither be met at the avoided crossing nor detuned from it. As a consequence, the decay rate $\Gamma_{\|}$ will be reduced by a factor

$$\left| \frac{1}{1 + i(\delta - 2\epsilon)/\kappa} \right| \tag{4.2}$$

compared with the full cavity-enhanced value. In this case the transition rate is strongly suppressed even at the avoided crossing and will not lead to significant decay inside the cavity.

The second case is $\delta < 2\epsilon$. As can be seen from Fig. 6(b), there is no longer a single detuning Δ_1, at which the cavity is resonant with a Floquet transition. Instead, cavity enhancement now occurs at two distinct frequencies, roughly symmetric to the avoided crossing. They can be obtained graphically by determining the intersections of the quasienergy ϵ with the line $\delta/2$ [Fig. 6(a)]. The fact that the peaks of cavity enhancement, on the one hand, and coupling between the Floquet levels, on the other, no longer coincide leads to a substructure of the total decay rate $\Gamma_{\|}$. In the example of Fig. 6, the single peak in the transition matrix element [Fig. 6(c)] and the double peaks in the cavity resonance [Fig. 6(b)] lead to the triplet shape of $\Gamma_{\|}$ shown in Fig. 6(d).

Depending on the width of the avoided crossing and the size of δ, other line shapes can occur. Some typical examples are shown in Fig. 7. Again, the contribution of the cavity resonance and the coupling between the Floquet levels are shown separately to clarify the origin of the structure in $\Gamma_{\|}$. It is apparent that the width of the resonances in the transition matrix element decreases inversely proportionally to the level splitting at the corresponding avoided crossing [Fig. 7(c)]. This leads to extremely sharp lines as the cavity resonance is approached. The change in the double peak structure of the resonance denominator [Fig. 7(b)] is less dramatic, as long as the resonance condition $\delta = 2\epsilon$ can be fulfilled. Otherwise there is only a broad single peak with a decreased amplitude. The resulting cavity-induced decay rate is presented in Fig. 7(d). At $\Delta_1 - \Delta_c \approx -9\kappa$, where the cavity is not resonant with any Floquet transition, cavity enhancement is negligible and only marginally increased decay is found. At $\Delta_1 - \Delta_c \approx -7.5\kappa$, two cavity resonances appear, split by an amount comparable to the width of the Floquet coupling peak. In this situation $\Gamma_{\|}$ also features two peaks. When the resonance in the coupling narrows more and more, the transition matrix element at the two cavity-supported frequencies gradually decreases and cavity enhancement becomes less important. At $\Delta_1 - \Delta_c \approx -6.3\kappa$, for example, the two cavity

enhanced peaks are not larger than the central peak at the avoided crossing. This results in the triplet structure from Fig. 6. As the size of the avoided crossing shrinks further, the amplitude of the outer maxima quickly decreases ($\Delta_1 - \Delta_c \approx -5.5\kappa$) until only the narrow central peak in the transition probability contributes. Enlarged views of the consecutive resonances are provided in Fig. 8, illustrating the relation between the peaks in $\Gamma_{\|}$ and the local structure of the Floquet levels.

Figures 7 and 8 were obtained for different resonances of the decay rate, distinguished by the number of driving field photons involved. The transition from cavity suppression to cavity enhancement of a Floquet resonance can be studied at a single avoided crossing if one of the experimental parameters, for example Δ_2, is varied. The result is presented in Fig. 9. The decay rate shows a pronounced maximum, corresponding to detunings such that cavity enhancement and an avoided crossing of the Floquet levels coincide. This is in keeping with the condition derived above for a strong resonance. By decreasing the detunings Δ_1 or Δ_2 one can observe the expected splitting, while at the same time the size of the decay rate goes to zero. In the opposite case of increasing detunings, the size of the resonance decreases too due to cavity suppression. Similar results are obtained if instead of the detunings the intensities of the driving fields are varied.

B. Intensity-dependent shift of the resonances

It is evident that only the strongest peaks in the decay rate will be relevant to the experiment, as a small decay rate does not lead to an observable change of the atomic population during the interaction time of atoms

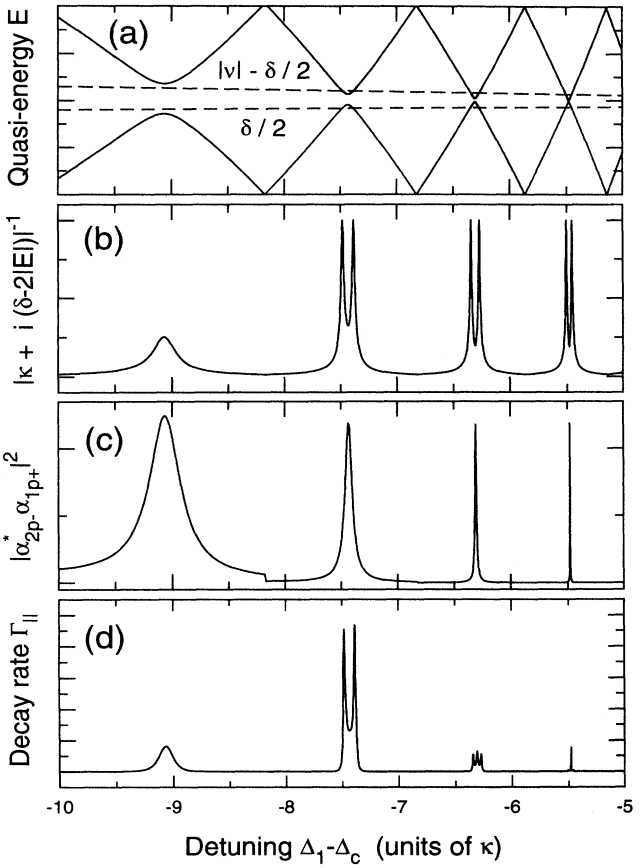

FIG. 7. Resonances in the decay rate $\Gamma_{\|}$ at four adjacent avoided crossings (see Fig. 6 for an explanation). The parameters are the same as those of Fig. 4.

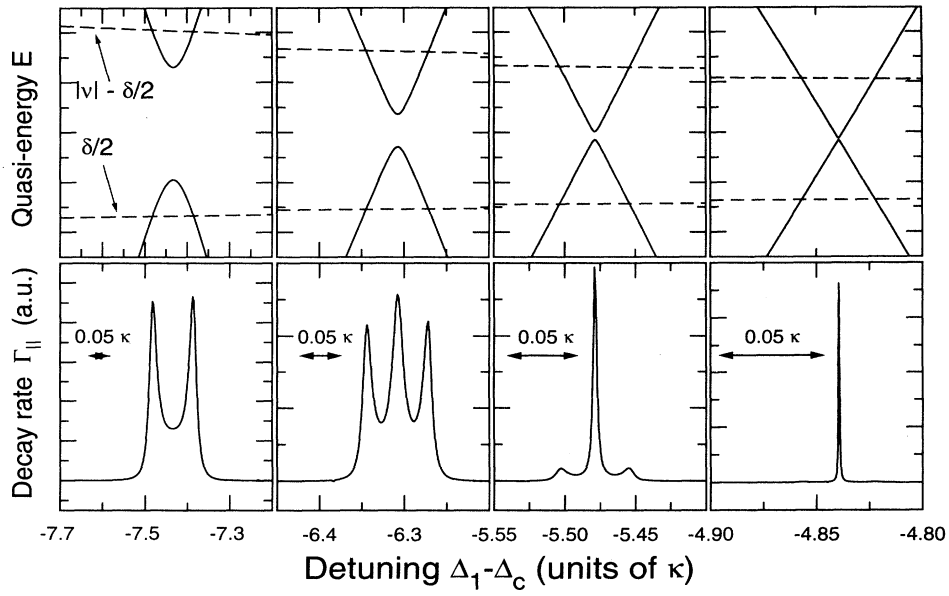

FIG. 8. Enlarged view of the avoided crossings and resonances in the decay rate from Fig. 7, exemplifying various possible line shapes and their relation to the structure of the avoided crossing.

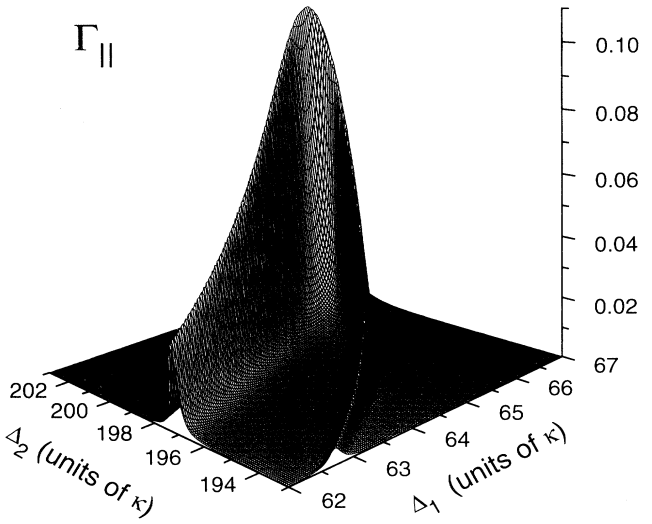

FIG. 9. Single resonance of $\Gamma_{||}$ in the Δ_1, Δ_2 plane. The maximum in the decay rate is reached when a Floquet transition becomes resonant with the cavity precisely at an avoided crossing. Parameters: $\Omega_1^0 = 3270\kappa$, $\Omega_2^0 = 53\,440\kappa$, and $\Delta_c = 80\kappa$.

and cavity field. Figure 10 shows a typical example, where only one peak significantly contributes to decay, while the other resonances are suppressed by the cavity. As shown in Sec. V, large isolated maxima in the decay rate $\Gamma_{||}$ correspond very well to the resonances observed experimentally.

In this section, we will focus on the large peaks in the decay rate, such as those of Figs. 9 and 10, occurring when the cavity is resonant with a Floquet transition at an avoided crossing. Specifically, the shift of these resonances as a function of the intensities of the driving fields will be discussed.

Again, we start by studying the shift of cavity enhancement and that of the avoided crossings separately. According to Eq. (3.15), for $\Delta_1 > \Delta_c$ and $P = 2$ maximum cavity enhancement occurs for

$$\delta + 2\epsilon + 2\nu = 0. \tag{4.3}$$

In Fig. 11(a) this relation is evaluated as a function of the detuning Δ_1 of the first driving field and its intensity Ω_1^0 (solid lines). In the same plot, the positions of the avoided crossings of the Floquet levels are represented by dashed lines. In keeping with the results obtained above, large decay is expected where the two sets of lines intersect. This is indeed the case, as can be seen by comparison with Fig. 11(b), showing the decay rate $\Gamma_{||}$ as a density plot.

For small values of Ω_1^0, the intensity-dependent shifts of cavity and avoided crossings are quite different, so that large maxima can appear only locally. With increasing field strength, however, the shift of the two quantities coincides in a larger region. Finally, the peaks in the decay rate split and the cavity gets out of resonance with the strong Floquet transition at the avoided crossing.

Figure 12 shows again a density plot of the decay rate $\Gamma_{||}$ as a function of the detuning ω_1 and the amplitude Ω_1^0 of the first driving field component over a large range.

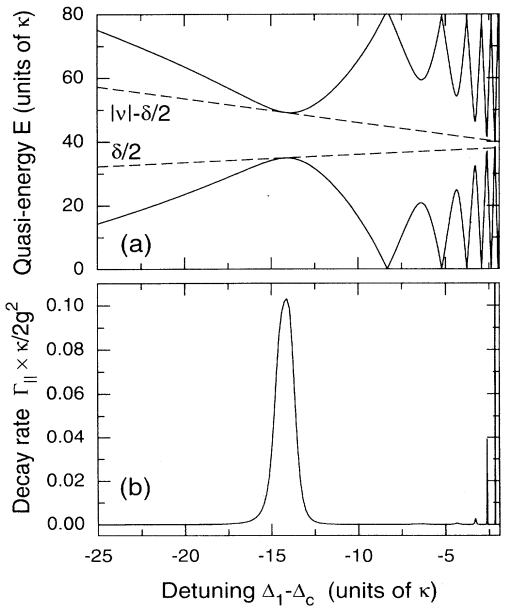

FIG. 10. Spectrum of $\Gamma_{||}$ showing one peak dominating the decay rate. At other avoided crossings transitions between the Floquet states are suppressed by the cavity. Parameters: $\Omega_1^0 = 2500\kappa$, $\Omega_2^0 = 60\,000\kappa$, $\Delta_2 = 254\kappa$, and $\Delta_c = 100\kappa$.

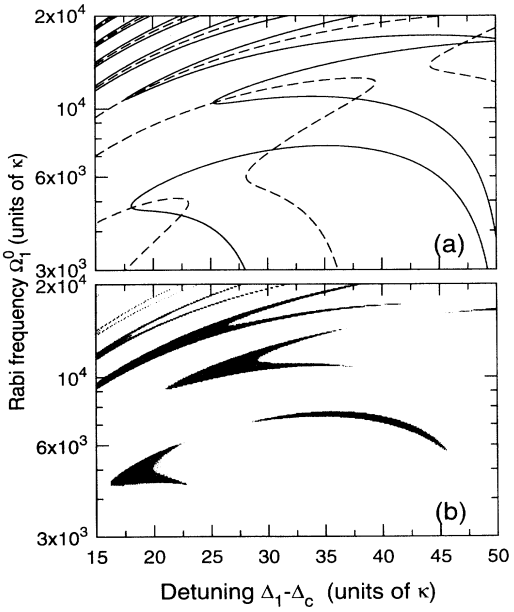

FIG. 11. (a) Cavity resonances for $P = 2$ (solid lines) and avoided crossings of the Floquet levels (dashed lines) for varying amplitudes of the first driving field. (b) Density plot of $\Gamma_{||}$. The dark regions, indicating a large decay rate, coincide with intersections of the curves in (a). Parameters: $\Omega_2^0 = 60\,000\kappa$, $\Delta_2 = 254\kappa$, and $\Delta_c = 100\kappa$.

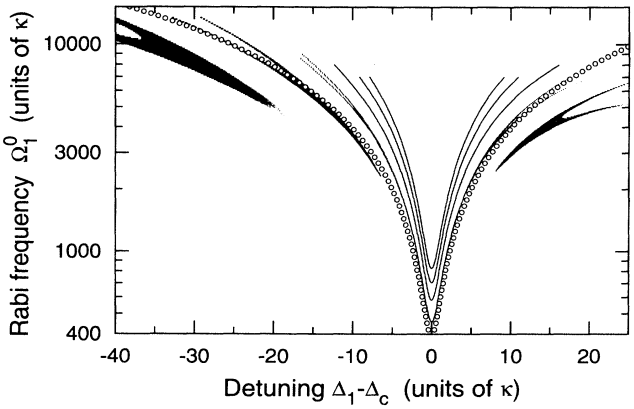

FIG. 12. Density plot of $\Gamma_{\|}$ as a function of the detuning and the amplitude of the first driving field. As the field strength is increased, the maximum decay rate slowly shifts to the outer (lower order) resonances. This behavior corresponds exactly to the empirical condition (5.2) for the center of the experimentally observed lines if the factor f is chosen as 2.35. The resulting empirical curve is represented by small circles. Parameters: $\Omega_2^0 = 20\,000\kappa$, $\Delta_2 = 200\kappa$, and $\Delta_c = 80\kappa$.

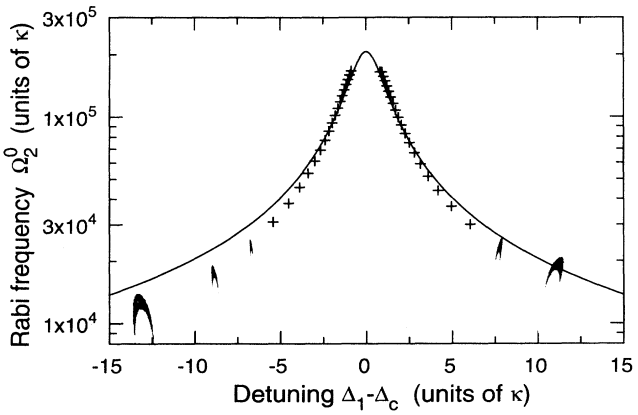

FIG. 13. Density plot of $\Gamma_{\|}$ as a function of the detuning of the first driving field and the amplitude of the second (fixed frequency) field. As Ω_2^0 is increased, decay occurs at resonances of increasing order, closer to the cavity frequency. As the higher-order resonances are too narrow to be resolved, maxima in the decay rate are marked by crosses for clarity. The solid line shows the empirical result (5.2) for $f = 1.9$. Parameters: $\Omega_1^0 = 3270\kappa$, $\Delta_2 = 200\kappa$, and $\Delta_c = 80\kappa$.

Generally, with increasing intensity, the strength of a given resonance in $\Gamma_{\|}$ slowly diminishes. Simultaneously the contribution of the neighboring resonance, further away from the cavity frequency, increases, so that effectively the center of gravity of the peaks in the decay rate slowly shifts to larger detunings from the cavity line. In the experiment always the largest resonance should be detected.

This agrees precisely with the observed behavior. Section V shows that the experimental peaks follow a certain curve, which is represented by small circles in Fig. 12. At small intensities, this curve coincides with the calculated intensity-dependent shift of the resonances. At larger field strengths, the curve interpolates very well the dominant peaks in $\Gamma_{\|}$.

Figure 13, on the other hand, shows the behavior of the decay rate when the amplitude Ω_2^0 of the second driving field with a fixed frequency is varied. In this situation a different structure of the decay rate is found. As the intensity is increased, the system does not follow a certain resonance, but jumps to a neighboring avoided crossing closer to the cavity center, which corresponds to a larger number of photons involved in the transition. The higher-order resonances become increasingly narrow until they cannot be resolved any more. Therefore, the location of the corresponding maxima in Fig. 13 is marked by crosses. The solid line is the experimental curve presented in Sec. V. The agreement between the experimentally determined shifts of the resonances and the calculated behavior of $\Gamma_{\|}$ confirms the central role of cavity-enhanced transitions among Floquet states in the system under study.

C. Effects of inhomogeneous broadening

Finally, we briefly discuss the effects of inhomogeneous broadening on the transition rates among Floquet states. The problem is again solved numerically. In Rydberg atom experiments, the main source of inhomogeneous broadening are Stark shifts from electric stray fields. As a simplification we assume that a given atom experiences a constant Stark shift during interaction with the cavity field. In this case the decay rate $\Gamma_{\|}$ may be calculated for a fixed atomic frequency. Afterwards an average over a Gaussian distribution of frequencies is taken to obtain an estimate of the decay rate in the presence of inhomogeneous broadening.

In Fig. 14(a) the decay rate $\Gamma_{\|}$ is shown as a function of the frequency shift of the atomic line. The decay rate is again represented as a density plot. With the exception of the two broad outer peaks, the position of the resonances changes little as the atomic frequency is varied. This is not surprising since the structure of the Floquet levels is governed by light shifts and only marginally depends on the energy separation of the unperturbed atomic states involved.

Weighting the results with a Gaussian of width w and integrating over the atomic frequency shift, we obtained the inhomogeneously broadened spectra compiled in Fig. 14(b). In this example there is only small broadening and practically no shift of the resonances, even if the inhomogeneous width w is as large as 50κ. This explains why in the experiment narrow lines were observed in spite of the presence of substantial inhomogeneous broadening.

Figure 15 shows an example of a broadened atomic line leading to additional structure in the decay rate. This is the case when, due to inhomogeneous broadening, the transition frequencies for a subset of atoms are shifted such that condition (3.15) is fulfilled. As a consequence, strong decay occurs and a second maximum appears, which may become larger than the original peak in the absence of inhomogeneous broadening. In this way, broadening of the atomic line can offer the system a wider range of possibilities to undergo cavity-enhanced decay,

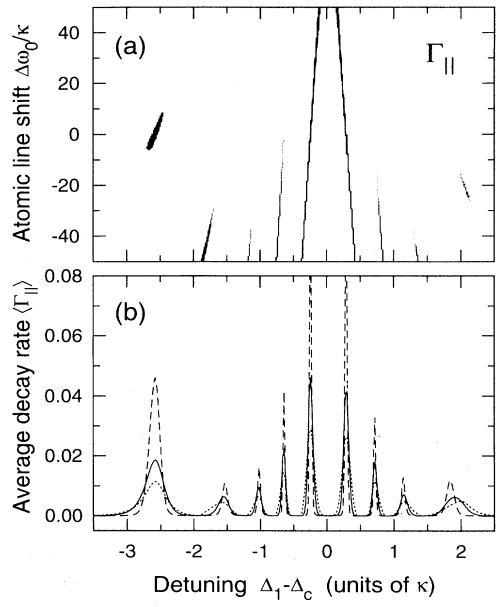

FIG. 14. (a) Density plot of $\Gamma_{||}$ as a function of the detuning Δ_1 of the first driving field and the shift $\Delta\omega_0 = \langle\omega_0\rangle - \omega_0$ from the average atomic frequency. (b) Spectra of $\Gamma_{||}$ for inhomogeneous broadening of width $w = 10\kappa$ (dashed line), $w = 30\kappa$ (solid line), and $w = 50\kappa$ (dotted line). Parameters: $\Omega_1^0 = 500\kappa$, $\Omega_2^0 = 16\,000$, $\Delta_2 = 200\kappa$, and $\Delta_c = 140\kappa$.

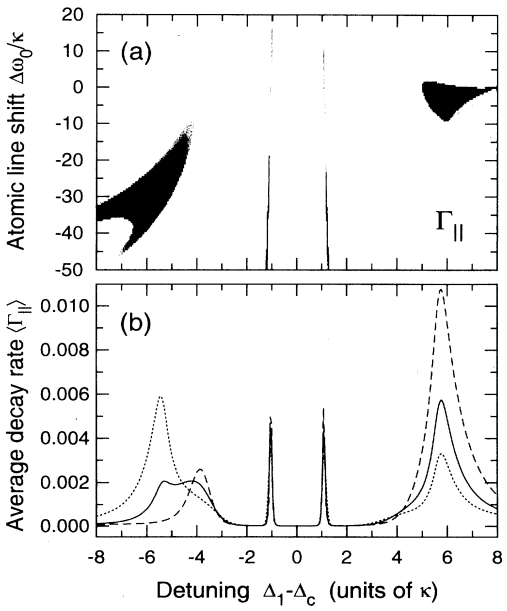

FIG. 15. (a) Same as Fig. 14(a). (b) Spectra of $\Gamma_{||}$ for inhomogeneous broadening of width $w = 10\kappa$ (dashed line), $w = 27\kappa$ (solid line), and $w = 50\kappa$ (dotted line). At $\Delta_1 - \Delta_c = -6\kappa$ a second peak appears due to cavity enhancement for a subset of detuned atoms. Parameters: $\Omega_1^0 = 400\kappa$, $\Omega_2^0 = 14\,440$, $\Delta_2 = 250\kappa$, and $\Delta_c = 100\kappa$.

thereby decreasing the separation between neighboring resonances in the spectra. It should be noted, however, that the inner resonances in Fig. 15 remain largely unaffected by broadening.

V. COMPARISON WITH EXPERIMENTAL OBSERVATIONS

The numerical results of Sec. IV provide an interpretation of recent experiments with Rydberg atoms in a moderate-Q cavity driven by a strong bichromatic field [16]. This section is devoted to a comparison between theory and experimental findings.

A schematic of the setup employed is shown in Fig. 16. The experiments are performed using a beam of ^{85}Rb atoms excited to the $53\,^2P_{3/2}$ Rydberg state. The atoms traverse a cylindrical microwave cavity along its axis. The TM_{020} mode of the cavity is tuned close to resonance with the $53\,^2P_{3/2} \rightarrow 53\,^2S_{1/2}$ transition ($\omega_0 = 2\pi \times 25.590\,03$ GHz) and driven by two separate microwave synthesizers whose frequency and output intensity may be controlled independently. The atom-field coupling g is $2\pi \times 17$ kHz, the cavity damping κ is $2\pi \times 6.7$ kHz. At a temperature of 4.2 K the thermal field in the TM_{020} mode corresponds to a mean photon number $\overline{n} = 2.9$.

The coupling of the bichromatically driven atoms to the vacuum field or the thermal field in the cavity leads to spontaneous decay as well as thermally induced transitions. In contrast to the optical domain, the emitted radiation cannot be observed directly, owing to the closed cavity geometry. The quantity monitored instead is the fraction P_2 of atoms leaving the cavity in the lower state ($53\,^2S_{1/2}$). For adiabatic entry and exit, there is a simple connection between P_2 and the decay rate $\Gamma_{||}$:

$$P_2 \sim \langle -|\rho|- \rangle \sim \left(1 - e^{-\Gamma_{||} T_{\rm int}}\right), \tag{5.1}$$

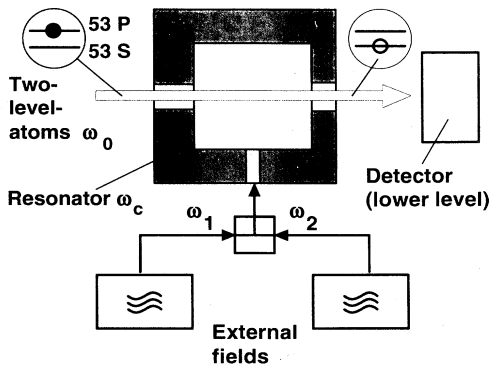

FIG. 16. Experimental setup. Atoms are prepared in the upper ($53\,^2P_{3/2}$) level before entering the cavity. Inside the cavity the atoms interact with the strong bichromatic driving field as well as the thermally occupied cavity mode. Outside the cavity the population of the lower atomic level ($53\,^2S_{1/2}$) is probed by state-selective field ionization.

where $T_{\rm int}$ is the interaction time of atoms and cavity mode and $|-\rangle$ is the lower Floquet basis state as defined in Eq. (2.17). Spectral information on the atom-cavity system is obtained by recording the lower level occupation P_2 as a function of the driving field frequencies. It is convenient to vary only the first driving field (ω_1), keeping all other parameters fixed.

Expression (5.1) shows that a substantial change in the lower level occupation can only occur if the rate $\Gamma_{||}$ exceeds the inverse transit time. This requirement is fulfilled by the strong resonances appearing when cavity enhancement coincides with a Floquet transition.

Another limitation is the finite experimental resolution. If the width of the resonances drops below the linewidth of the microwave source employed, detection is no longer possible. As the width of the peaks decreases with the number of photons involved in the transition (cf. Fig. 7), there is an upper boundary to the multiphoton order N that can be resolved experimentally. In Ref. [16] resonances up to $N = 37$ could be observed (see Fig. 19).

According to these theoretical considerations, spectra should be dominated by a single pair of resonances when the frequency ω_1 is tuned across the cavity resonance. All other resonances are either suppressed by the cavity or too narrow to be resolved. This is precisely confirmed by the experimental results, a typical example being presented in Fig. 17(a). For comparison, Fig. 17(b) shows the corresponding theoretical calculation of P_2 as a function of the detuning of the first driving field. Both curves are approximately symmetrical with respect to the cavity frequency.

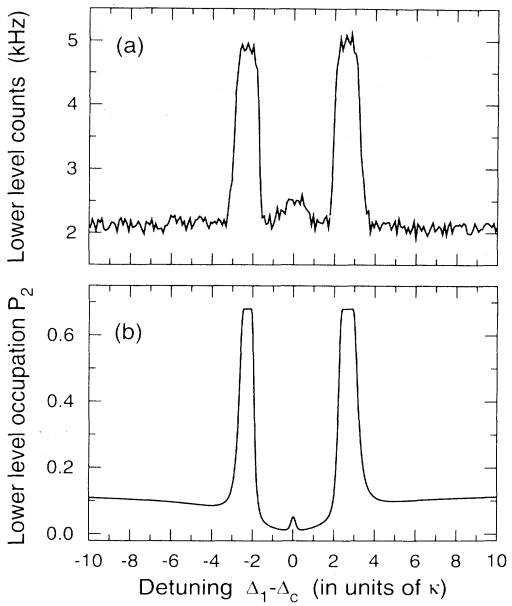

FIG. 17. Resonances in the lower level occupation as a function of the frequency of the first driving field. (a) Experimental result. Parameters: $\Omega_1^0 = 120$ MHz; $\Omega_2 = 15$ MHz; $\omega_2 - \omega_c = 2\pi \times 1018$ kHz; $\omega_c - \omega_0 = 2\pi \times 681$ kHz. (b) Corresponding theoretical calculation. The best agreement with the experiment is obtained for $\kappa \approx 2\pi \times 21$ kHz.

A striking property of the resonances in Fig. 17 is their line shape, characterized by steep edges and a flat portion in the middle. The fact that the occupation of the atomic levels does not change in a finite range of driving field frequencies signifies that cavity-induced decay is strong enough to achieve thermalization of the Floquet population inside the cavity. It is important to note that it is the Floquet states that are pumped by the vacuum or the thermal field in the cavity. This leads to a significantly higher population in the lower *unperturbed* atomic level (P_2=68%) than the thermal equilibrium value (P_2=57%).

The experimental peaks are wider than theoretically predicted because of inhomogeneous broadening, which has not been included in the calculations. Inhomogeneous broadening also washes out most of the substructure of the resonances discussed in Sec. IV A. However, even in the presence of inhomogeneous broadening, remarkable small linewidths are measured, in keeping with the numerical investigations of Sec. IV C. Figure 18 shows a pair of resonances only 1 kHz wide, which is narrower than the cavity linewidth and the inverse transit time of the atoms.

Interestingly, driving field parameters can be found, for which several pairs of resonances appear in the experimental spectra. An example is shown in Fig. 19. As indicated in the figure, the inner narrow resonances correspond to a much higher multiphoton order than the broad outer peaks. The decreasing width of the resonances towards the cavity frequency is in agreement with the theoretical prediction for the decay rate $\Gamma_{||}$ as can be seen from Fig. 7.

In Sec. IV B the dependence of the multiphoton resonances on the intensities of the driving fields was calculated. To experimentally test the numerical results, ω_1 spectra were recorded for different values of the strength of the field component at ω_1. The frequency and strength of the second driving field were kept constant. Results for a single pair of resonances are compiled in Fig. 20. The splitting of the two peaks increases with the intensity of the first driving field. The position of the observed resonances obeys a simple empirical condition: An increase in the driving field amplitude E_1 shifts the resonance

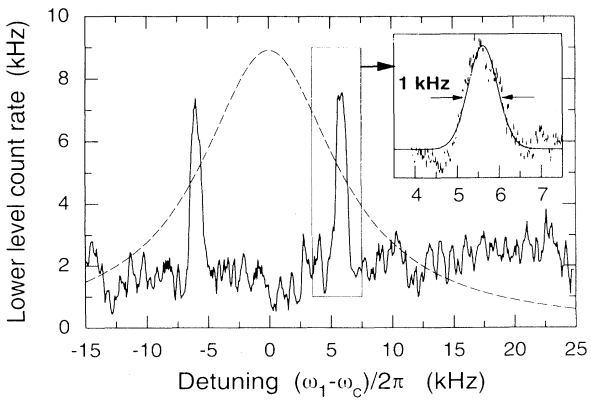

FIG. 18. Narrow resonances in the lower level occupation. The dashed line represents the cavity response function.

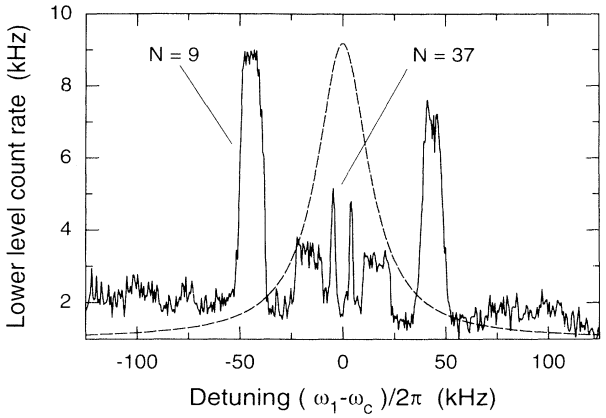

FIG. 19. Lower level count rate as a function of ω_1. Several multiphoton resonances are observed. The order of the two most prominent pairs of resonances is indicated. The dashed line represents the cavity resonance. Parameters: $\omega_2 - \omega_c = 2\pi \times 1300$ kHz and $\omega_c - \omega_0 = 2\pi \times 937$ kHz.

frequency ω_1^{res} in such a way that the intracavity Rabi frequency Ω_1, defined in Eq. (2.8), stays constant.

The shift of the resonance frequencies in the ω_1 spectra is different, when the intensity of the field component at ω_2 is varied. According to Fig. 21, the splitting of the peaks decreases when the strength of the second driving field is increased. The shift observed in the experiment is descibed by an extension of the empirical condition above: Peaks in the decay rate appear when the intracavity Rabi frequencies Ω_1 and Ω_2 are equal up to a constant factor f of the order of unity. Using Eq. (2.8), this can be written as

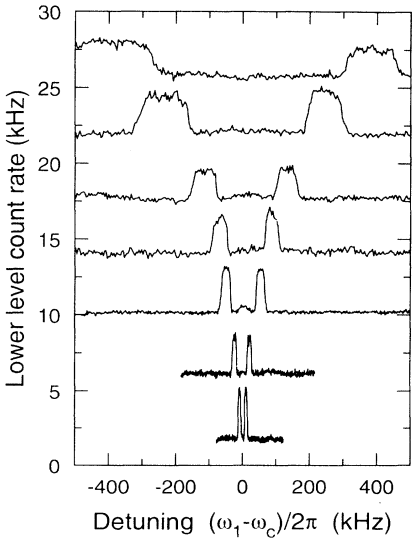

FIG. 20. Lower level count rate as a function of ω_1 for different intensities of the first driving field. Starting from the lowest trace, the field strength increases by a factor of 10, successively. Detunings $\omega_2 - \omega_c = 2\pi \times 1700$ kHz and $\omega_c - \omega_0 = 2\pi \times 680$ kHz.

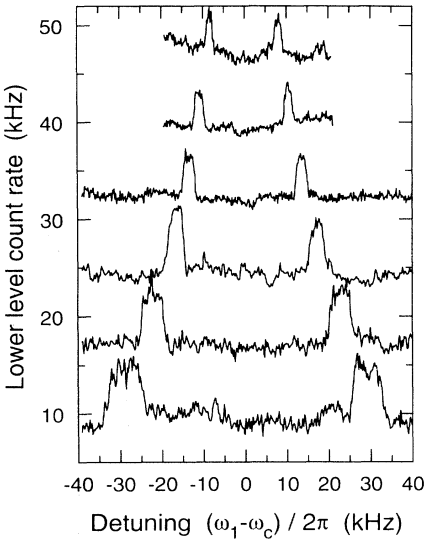

FIG. 21. Lower level count rate as a function of ω_1 for different intensities of the second driving field. Starting from the lowest trace, the field strength increases by a factor of 2.5, successively. Detunings: $\omega_2 - \omega_c = 2\pi \times 1700$ kHz; $\omega_c - \omega_0 = 2\pi \times 680$ kHz.

$$\left|\frac{\Omega_1^0}{\kappa + i(\omega_c - \omega_1)}\right| = f \times \left|\frac{\Omega_2^0}{\kappa + i(\omega_c - \omega_2)}\right|. \qquad (5.2)$$

Figures 12 and 13 demonstrate that condition (5.2) interpolates the numerically obtained maxima in the decay rate very well. In Fig. 12 the empirical condition, represented by small circles, follows a certain multiphoton resonance for a large range of input intensities of the first field before crossing over to a stronger neighboring resonance. In Fig. 13 the empirical condition (solid line) again quite accurately describes the position of maxima in the decay rate when the intensity of the second field is varied.

The quantitative agreement between the experimentally determined shifts of the resonances and the calculated behavior of $\Gamma_{||}$ confirms that the bichromatically driven system is best described by Floquet states interacting with the vacuum field of the cavity.

VI. SUMMARY

In conclusion, we have provided a theoretical framework for studying the dynamics of Rydberg atoms in a bichromatic field in the bad cavity limit, where the cavity field adiabatically follows the atomic dynamics. From this we have derived an expression for the decay rate of the population inversion in the Floquet basis. Calculating the transition rates for a large range of parameters of the bichromatic field, we have obtained good agreement with the spectra observed experimentally. In particular, the sharp resonances found in the spectra have a natural interpretation in our model as cavity-induced decay of Floquet states. Furthermore, we have been able to explain how the structure of the resonances is modified

by changes in the Rabi frequencies of the applied fields, confirming the empirical condition that resonances appear whenever the intracavity Rabi frequencies have a certain constant ratio of the order of unity. We have demonstrated that for a certain range of parameters the resonances in the transition rates may become extremely narrow, even in the presence of inhomogeneous broadening. Again, this is in agreement with experiments.

Finally, we should mention that we have not exhausted all the possibilities that can occur in cavity quantum electrodynamics in the presence of bichromatic driving fields. Dynamic effects in high-Q cavities such as the oscillatory exchange of energy between atom and cavity field as well as cooperative effects can only be addressed in the future.

Note added. While this work was being completed, P. Lambropoulos and M. Elk [23] had also examined the response of a two-level system driven by a strong bichromatic field in a cavity. They developed a numerical method to treat the interaction between the cavity-field and the atom without the Born approximation.

[1] B. R. Mollow, Phys. Rev. **188**, 1969 (1969).
[2] A. Bonch-Bruevich, T. Vartanyan, and N. A. Chigir, Zh. Eskp. Teor. Fiz. **77**, 1899 (1979) [Sov. Phys. JETP **50**, 901 (1979)].
[3] S. Chakmamjian, K. Koch, and J. C. R. Stroud, J. Opt. Soc. Am. B **5**, 2015 (1988).
[4] F. Y. Wu, R. E. Grove, and S. Ezekiel, Phys. Rev. Lett. **35**, 1426 (1975).
[5] W. Hartig, W. Rasmussen, R. Schieder, and H. Walther, Z. Phys. A **278**, 205 (1976).
[6] Y. Zhu *et al.*, Phys. Rev. A **41**, 6574 (1990).
[7] G. S. Agarwal, Y. Zhu, D. J. Gauthier, and T. W. Mossberg, J. Opt. Soc. Am. B **8**, 1163 (1991).
[8] E. M. Purcell, Phys. Rev. **69**, 681 (1946).
[9] D. J. Heinzen, J. J. Childs, J. E. Thomas, and M. S. Feld, Phys. Rev. Lett. **58**, 1320 (1987).
[10] P. Goy, J. M. Raimond, M. Gross, and S. Haroche, Phys. Rev. Lett. **50**, 1903 (1983).
[11] R. G. Hulet, E. S. Hilfer, and D. Kleppner, Phys. Rev. Lett. **55**, 2137 (1985).
[12] W. Jhe *et al.*, Phys. Rev. Lett. **58**, 666 (1987).
[13] M. Lewenstein, T. W. Mossberg, and R. J. Glauber, Phys. Rev. Lett. **59**, 775 (1987).
[14] W. Lange and H. Walther, Phys. Rev. A **48**, 4551 (1993).
[15] Q. Wu, D. J. Gauthier, and T. W. Mossberg, Phys. Rev. A **49**, R1519 (1994).
[16] W. Lange, H. Walther, and G. S. Agarwal, Phys. Rev. A **50**, R3595 (1994).
[17] G. Floquet, Ann. l'Ecole Norm. Sup. **12**, 47 (1883).
[18] F. H. M. Faisal, *Theory of Multiphoton Processes*, *Physics of Atoms and Molecules* (Plenum, New York, 1987), Chap. 10.
[19] D. R. Dion and J. O. Hirschfelder, in *Advances in Chemical Physics*, edited by I. Prigogine and S. A. Rice (Wiley, New York, 1976), Vol. XXXV, pp. 265–350.
[20] M. Allegrini, E. Arimondo, and A. Bambini, Phys. Rev. A **15**, 718 (1977).
[21] G. S. Agarwal, W. Lange, and H. Walther, Phys. Rev. A **48**, 4555 (1993).
[22] J. H. Shirley, Phys. Rev. **138**, B 979 (1965).
[23] M. Elk and P. Lambropoulos, Phys. Rev. A **50**, 1490 (1994).

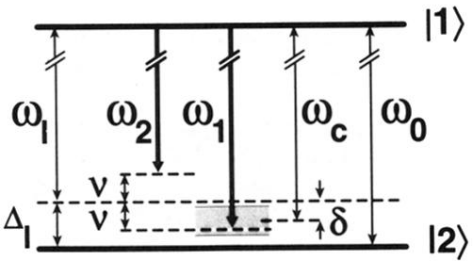

FIG. 1. Scheme of the unperturbed atomic states and the frequencies characterizing the system. The theoretical analysis uses the frame rotating at the average driving frequency ω_l. Experimental spectra are taken by scanning ω_1 across the cavity frequency ω_c (shaded region) while keeping ω_2 fixed.

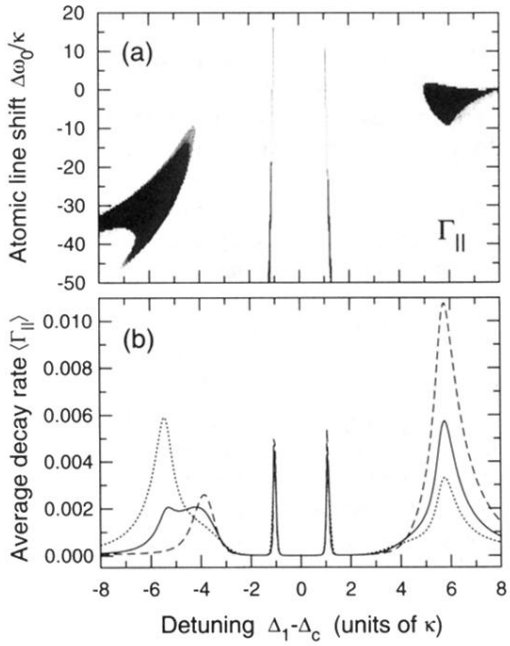

FIG. 15. (a) Same as Fig. 14(a). (b) Spectra of $\Gamma_{||}$ for inhomogeneous broadening of width $w = 10\kappa$ (dashed line), $w = 27\kappa$ (solid line), and $w = 50\kappa$ (dotted line). At $\Delta_1 - \Delta_c = -6\kappa$ a second peak appears due to cavity enhancement for a subset of detuned atoms. Parameters: $\Omega_1^0 = 400\kappa$, $\Omega_2^0 = 14\,440$, $\Delta_2 = 250\kappa$, and $\Delta_c = 100\kappa$.

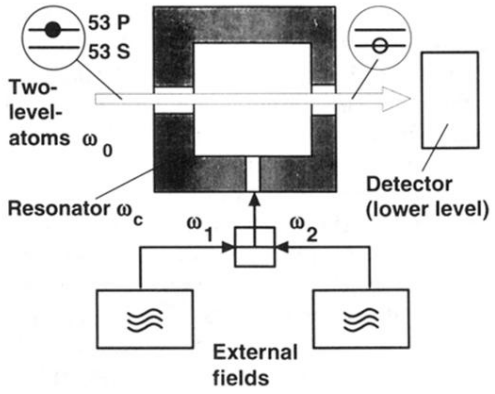

FIG. 16. Experimental setup. Atoms are prepared in the upper ($53\,^2P_{3/2}$) level before entering the cavity. Inside the cavity the atoms interact with the strong bichromatic driving field as well as the thermally occupied cavity mode. Outside the cavity the population of the lower atomic level ($53\,^2S_{1/2}$) is probed by state-selective field ionization.